



**HAL**  
open science

## **Cool episode and platform demise in the Early Aptian: new insights on the links between climate and carbonate production.**

Aurélie Bonin, Emmanuelle Pucéat, Emmanuelle Vennin, Emanuela Mattioli,  
Marcos Aurell, Michael Joachimski, Nicolas Barbarin, Rémi Laffont

### ► To cite this version:

Aurélie Bonin, Emmanuelle Pucéat, Emmanuelle Vennin, Emanuela Mattioli, Marcos Aurell, et al.. Cool episode and platform demise in the Early Aptian: new insights on the links between climate and carbonate production.. *Paleoceanography*, 2016, 31 (1), pp.66-80. 10.1002/2015PA002835 . hal-01284190

**HAL Id: hal-01284190**

**<https://hal.science/hal-01284190>**

Submitted on 1 Mar 2022

**HAL** is a multi-disciplinary open access archive for the deposit and dissemination of scientific research documents, whether they are published or not. The documents may come from teaching and research institutions in France or abroad, or from public or private research centers.

L'archive ouverte pluridisciplinaire **HAL**, est destinée au dépôt et à la diffusion de documents scientifiques de niveau recherche, publiés ou non, émanant des établissements d'enseignement et de recherche français ou étrangers, des laboratoires publics ou privés.

Copyright



## RESEARCH ARTICLE

10.1002/2015PA002835

## Key Points:

- Cooling evidenced during the late Early Aptian, postdating most of OAE1a
- Warmest interval coincides with OAE1a and microbialites development
- Change in neritic carbonate assemblages and in nannoconid size during cooling

## Correspondence to:

E. Pucéat,  
emmanuelle.puceat@u-bourgogne.fr

## Citation:

Bonin, A., E. Pucéat, E. Vennin, E. Mattioli, M. Aurell, M. Joachimski, N. Barbarin, and R. Laffont (2016), Cool episode and platform demise in the Early Aptian: New insights on the links between climate and carbonate production, *Paleoceanography*, 31, 66–80, doi:10.1002/2015PA002835.

Received 13 MAY 2015

Accepted 2 DEC 2015

Accepted article online 12 DEC 2015

Published online 16 JAN 2016

## Cool episode and platform demise in the Early Aptian: New insights on the links between climate and carbonate production

Aurélié Bonin<sup>1</sup>, Emmanuelle Pucéat<sup>2</sup>, Emmanuelle Vennin<sup>2</sup>, Emanuela Mattioli<sup>3</sup>, Marcos Aurell<sup>4</sup>, Michael Joachimski<sup>5</sup>, Nicolas Barbarin<sup>6</sup>, and Rémi Laffont<sup>2</sup>

<sup>1</sup>Badley Ashton and Associates Ltd., Horncastle, UK, <sup>2</sup>UBFC, UMR Biogéosciences 6282, Dijon, France, <sup>3</sup>UMR 5276 CNRS, LGLTPE, UCB Lyon 1, ENS Lyon, Lyon, France, <sup>4</sup>Departamento de Ciencias de la Tierra, Universidad de Zaragoza, Zaragoza, Spain, <sup>5</sup>Geozentrum Nordbayern, Universität Erlangen-Nürnberg, Erlangen, Germany, <sup>6</sup>CEREGE-UMR CNRS 6635, Dijon, France

**Abstract** The Early Aptian encountered several crises in neritic and pelagic carbonate production, major perturbations in the carbon cycle, and an oceanic anoxic event (OAE1a). Yet the causal links between these perturbations and climate changes remain poorly understood, partly because temperature records spanning the Early Aptian interval are still scant. We present new  $\delta^{18}\text{O}$  data from well-preserved bivalves from a carbonate platform of the Galve subbasin (Spain) that document a major cooling event postdating most of OAE1a. Our data show that cooling postdates the global platform demise and cannot have triggered this event that occurred during the warmest interval. The warmest temperatures coincide with the time equivalent of OAE1a and with platform biotic assemblages dominated by microbialites at Aliaga as well as on other Tethyan platforms. Coral-dominated assemblages then replace microbialites during the subsequent cooling. Nannoconids are absent during most of the time equivalent of the OAE1a, probably related to the well-known crisis affecting this group. Yet they present a transient recovery in the upper part of this interval with an increase in both size and abundance during the cool interval portion that postdates OAE1a. An evolution toward cooler and drier climatic conditions may have induced the regional change from microbial to coral assemblages as well as nannoconids size and abundance increase by limiting continent-derived input of nutrients.

### 1. Introduction

The Early Cretaceous period encountered several episodes of carbonate production crises, affecting both the pelagic and neritic domains [e.g., *Erba*, 1994; *Weissert et al.*, 1998; *Föllmi et al.*, 1994, 2006; *van Buchem et al.*, 2010]. A major crisis occurred during the late Early Aptian in the Tethyan realm and is associated with a globally recorded positive  $\delta^{13}\text{C}$  excursion following a brief negative spike potentially linked to increased volcanism [*Jenkyns and Wilson*, 1999; *Menegatti et al.*, 1998; *Weissert and Erba*, 2004; *Tejada et al.*, 2009]. The onset of the  $\delta^{13}\text{C}$  excursions coincides with widespread black shale deposition corresponding to oceanic anoxic event OAE1a [*Menegatti et al.*, 1998; *Méhay et al.*, 2009; *Tejada et al.*, 2009] and to the nannoconid crisis [*Erba*, 1994; *Erba and Tremolada*, 2004] inducing a drastic decline in fluxes of this rock-forming nannoplankton group.

The carbonate production crises occurred at a time of climate instability as evidenced by short-term (<1 Myr) fluctuations of marine surface temperatures [*Pucéat et al.*, 2003; *Steuber et al.*, 2005]. Both climate cooling and increased nutrient inputs have been suggested as potential factors to explain carbonate platform demise [e.g., *Weissert et al.*, 1998]. Conversely, recent modeling studies have proposed carbonate production crises as a possible trigger for short-lived cold interludes during the Jurassic and Cretaceous [*Donnadieu et al.*, 2011]. However, the causal link between climate and carbonate production remains unclear, mainly because reliable records of sea surface temperatures (SSTs) spanning these carbonate crises are still scant. Based on the  $\text{TEX}_{86}$  proxy, cold snaps have been identified in the Late Aptian prior to OAE1b, with the first one concomitant both to a decrease in planktonic foraminifera and nannoconids abundances and to carbonate platform-drowning events [*Weissert et al.*, 1998; *McAnena et al.*, 2013]. In the Early Aptian, records of upper ocean temperatures based on rudist or fish tooth  $\delta^{18}\text{O}$  [*Pucéat et al.*, 2003; *Steuber et al.*, 2005] suggest a cooling episode during the earliest Aptian. However, biostratigraphic calibration of the oxygen isotope records is not precise enough to identify a causal relationship between climate changes and carbonate

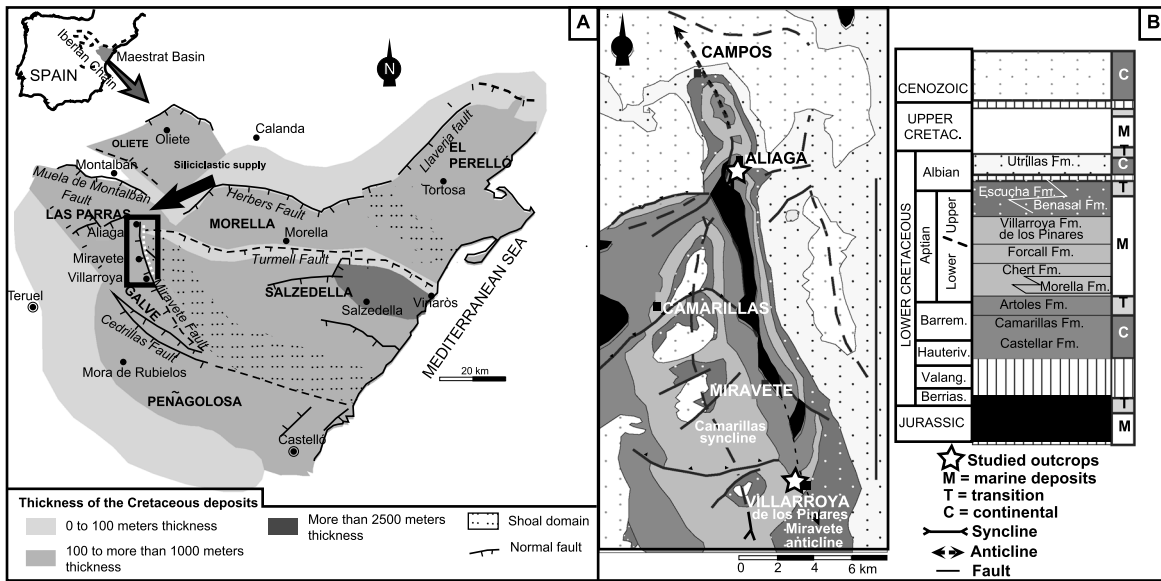


**Figure 1.** Detailed location of the studied sections in the (a) eastern Iberian Maestrat Basin and (b) geological settings of the Galve platform: simplified geological map and main Lower Cretaceous lithostratigraphic units. Modified from Embry et al. [2010].

production crises during this time interval. More recently, high-resolution records have been published for the Early Aptian but are mainly based on bulk rock  $\delta^{18}\text{O}$  composition, which can be sensitive to postdepositional alteration during diagenesis and to changes in coccolith assemblages as different vital effects in these organisms may affect the  $\delta^{18}\text{O}$  record [Dudley et al., 1986; Ando et al., 2008; Kuhnt et al., 2011; Keller et al., 2011]. Additional high-resolution SST records are based on the  $\text{TEX}_{86}$  proxy but are restricted to limited time intervals within OAE1a [Dumitrescu et al., 2006].

In this study we present a new sea surface (0–100 m) temperature record for the Early Aptian using the oxygen isotope ratios of stratigraphically well-dated bivalve shells (oysters and rudists). The samples have been recovered from two outcrops located in the Galve subbasin (northern Spain). Major biotic turnovers have been documented in these sections and correlated to similar events occurring throughout the Tethys during the Aptian [Embry et al., 2010]. Most importantly, unlike most neritic environments around the Tethys, the studied sections present continuous sedimentation, at basin scale, during most of the Early Aptian, spanning OAE1a and the associated biocalcification crisis. Thus, they provide the opportunity to study for the first time evolution of neritic and pelagic carbonate producers directly in regard to changes in seawater temperature.

## 2. Geological Setting

The Maestrat Basin results from a Late Jurassic–Early Cretaceous continental rifting that affected the Iberian Plate [Salas and Casas, 1993; Salas et al., 1991]. This extensional basin is a consequence of a progressive opening of the central Atlantic Ocean and the western Neotethys [Salas et al., 1991]. The Maestrat Basin was compartmentalized into seven subbasins, recording a kilometer-thick succession composed of mixed carbonate-siliciclastic deposits [Canérot et al., 1982]. During the late Eocene–early Miocene, the Maestrat Basin was tectonically inverted as a consequence of the Alpine compression [Liesa et al., 2006]. The two studied sections, Aliaga and Villarroya de los Pinares, are located in the Galve subbasin included in the Maestrat Basin (Figure 1).

## 3. Stratigraphic Context and Depositional Settings

The Aptian succession can be subdivided into four third-order sequences, the age of which was calibrated by ammonites, orbitolinids, and  $\delta^{13}\text{C}$  stratigraphy [Embry et al., 2010] (Figure 2). A negative spike is recorded at the top of the Forcall marls (equivalent to C3 according to Menegatti et al. [1998]) predating the positive carbon isotope excursion, allowing identification of OAE1a time equivalent [Embry et al., 2010] (Figure 2). Sedimentary environments range from continental or coastal domains to outer platform settings, with water

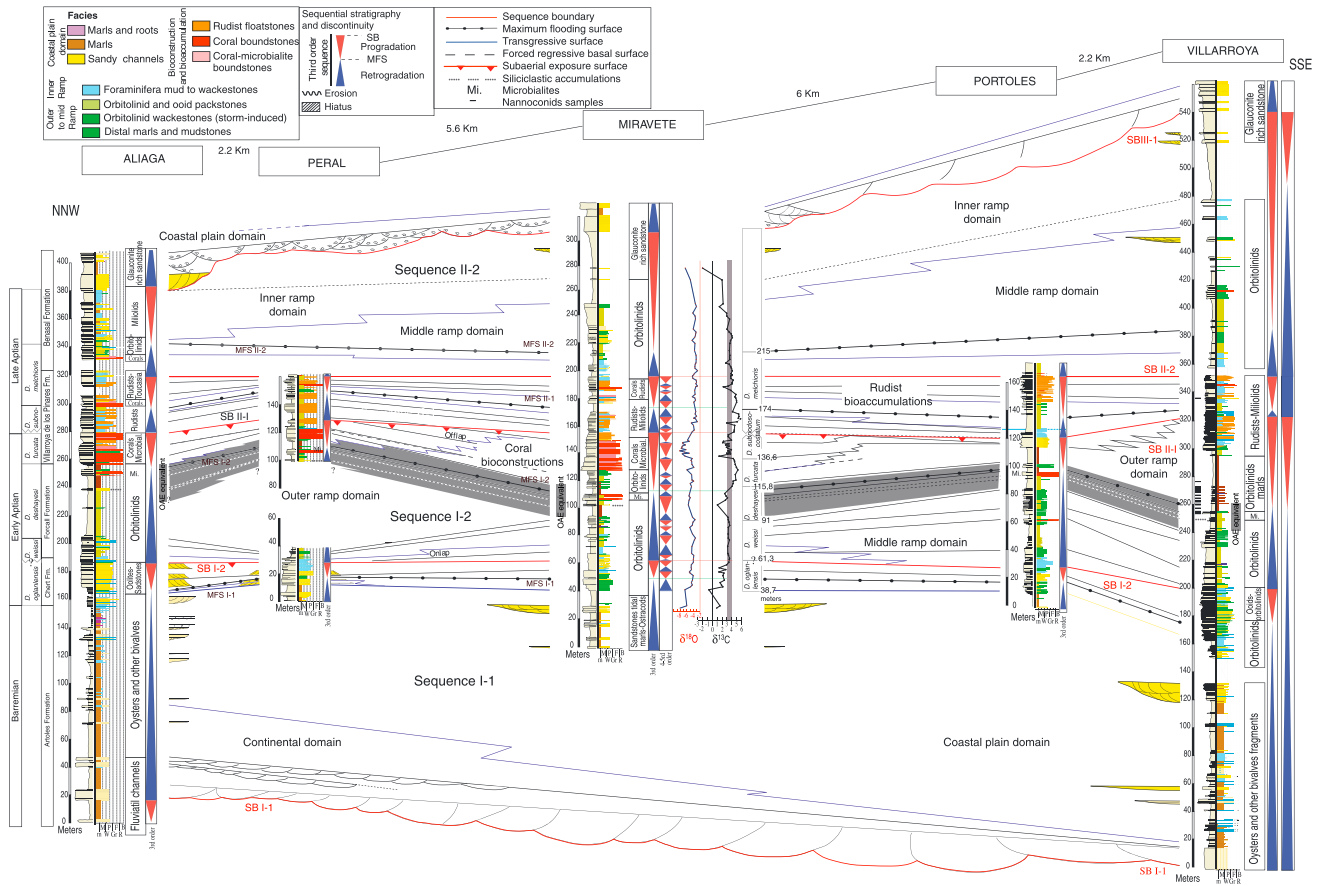


**Figure 2.** Stratigraphic model modified from Embry et al. [2010] and correlations based on foraminifera and ammonites for the Galve platform. The position of OAE1a as indicated on the Miravete section is based on the carbon isotope record available for this section [Embry et al., 2010] and includes the negative  $\delta^{13}\text{C}$  excursion as defined in Bover-Arnal et al. [2010] and has been extrapolated to the other sections through the stratigraphic correlations.

depths up to ~40 m deep at Aliaga and up to ~80 m deep at Villarroya de los Pinares (Figure 3). Facies evolution is associated with specific biotic associations replacement, with an evolution from an orbitolinid-dominated ramp to a microbialite-coral-dominated platform passing into a rudist-dominated ramp system and a return to an orbitolinid-dominated ramp [Embry et al., 2010] (Figures 2–4). While shallow-water carbonate systems along the northern Tethyan margin commonly record platform demise in the earliest Aptian (*D. weissi* Zone) [Arnaud et al., 1998; Föllmi and Gainon, 2008], carbonate platforms were growing on the southern Tethyan margin (Arabian Plate) up to the Early/Late Aptian and in the Galve subs basin up to the Aptian/Albian boundary due to both regional tectonic factors and eustatism [Embry et al., 2010; van Buchem et al., 2010; Bover-Arnal et al., 2010].

At Aliaga, where the bivalves analyzed for  $\delta^{18}\text{O}$  have been sampled, normal marine conditions are observed as evidenced by biotic assemblages (*Bacinnella-Lithocodium*, corals, and foraminifera) and sedimentary structures (megaripples, carbonate sandwaves, bioturbations, and storm-induced deposits), with the exception of the lowermost 160 m of the section that present washover deposits of an inner ramp domain. These lowermost 160 m are composed of coastal plain deposits interrupted by marine episodes illustrated by the presence of a stenohaline fauna such as echinoderms, foraminifera, green algae, and serpulids (for further details see the complete description in Embry et al. [2010]). All oysters sampled for oxygen isotope at the base of the section have been recovered from these levels recording normal salinity. After 160 m from the base of the section and up to about 205 m, the depositional environments correspond to upper to lower shoreface conditions, with a water depth up to 20 m [Vennin and Aurell, 2001]. The presence of foraminifera (orbitolinids), green algae, echinoderms, serpulids, and bryozoans indicates stenohaline conditions. From 205 m to about 250 m from the base of the section, slightly deeper conditions are recorded, indicated by upper offshore

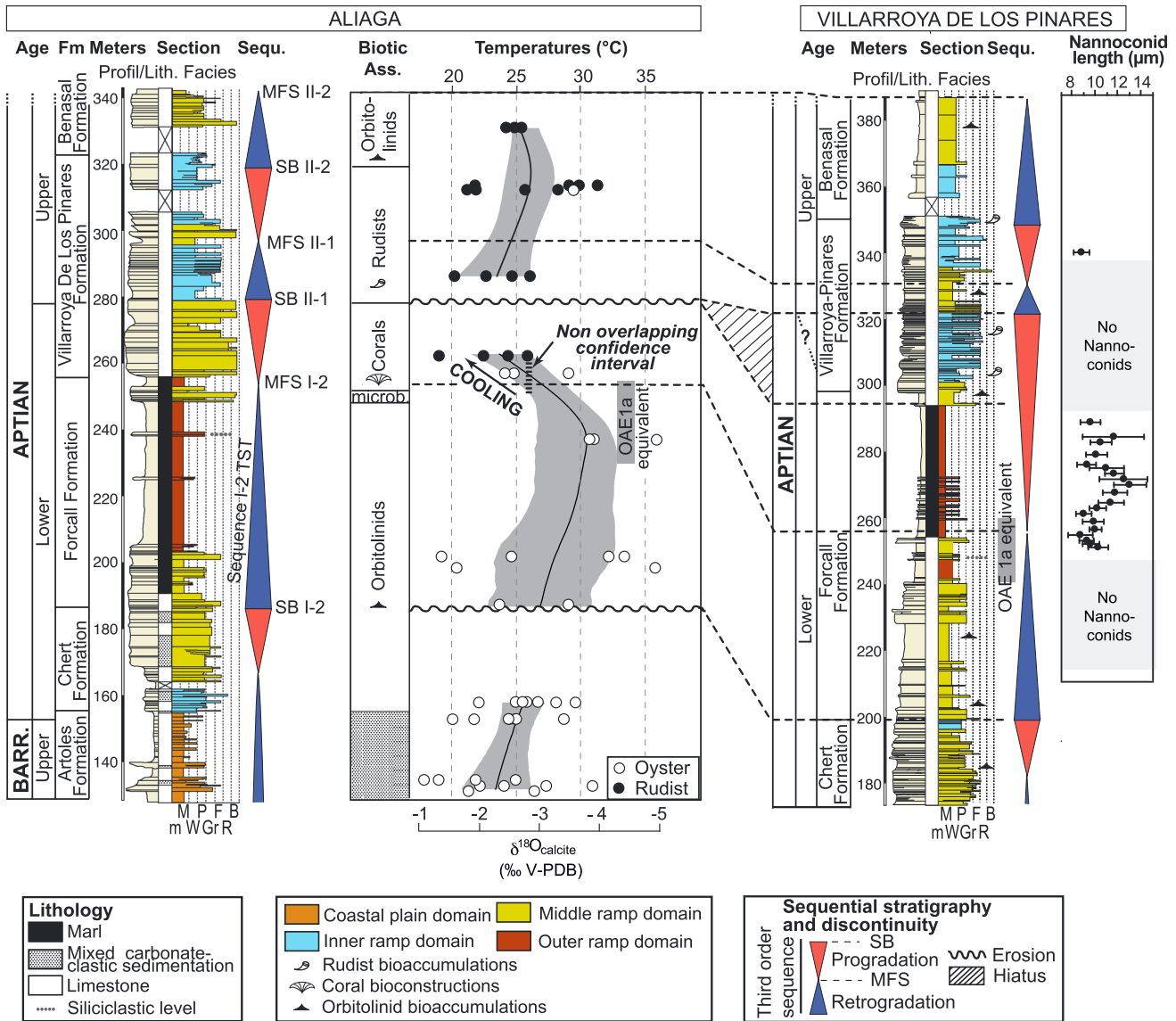


**Figure 3.** Oxygen isotope data from rudists (black circles) and oysters (white circles) plotted along the sedimentary succession at Aliaga and nannoconid length evolution along the Villarroya de los Pinares section (error bar = 95% confidence interval). Temperatures were calculated from bivalve  $\delta^{18}\text{O}$  using the equation of Anderson and Arthur [1983] and a  $\delta^{18}\text{O}_{\text{seawater}}$  of  $-0.7\text{‰}$  Vienna SMOW [Zhou et al., 2008]. Black curve fitting the  $\delta^{18}\text{O}$  data is a Kernel smoothed curve [e.g., Ruppert et al., 2003] with a 95% confidence interval (grey area) calculated by bootstrap (see text for more details). Sequential framework and facies analysis are modified from Embry et al. [2010]. Fm: formation; Lith.: lithology; MFS: maximum flooding surface; SB: sequence boundary; Sequ.: sequential analysis; and Biotic ass: biotic association. Facies: m = marl, M = mudstone, W = wackestone, P = packstone, Gr = grainstone, F = floatstone, R = rudstone, and B = boundstone.

environments dominated by storm-induced deposits, characteristic of a water depth typically around 40 m. Normal marine conditions are inferred from the presence of foraminifera (orbitolinids), ammonite fragments, echinoderms, and bivalves *Trigonia* sp. and *Neithea* sp. From 250 to 280 m, shallower depositional environments (10 to 40 m water deep) permit the installation of coral reefs. In this interval, *Bacinnella*, foraminifera, corals, stromatoporoids, echinoderms, and serpulids indicate open marine conditions. At about 280 m, sequence boundary II-1 (SB II-1) marks an important emersion event [Embry et al., 2010, p. 134, Figure 12]. The last bivalves sampled for isotope analyses were recovered from levels that are well below this sequence boundary (about 20 m). Above this sequence and up to the top of the succession, depositional settings remain shallow, in a shoreface domain dominated by rudists and foraminifera, typically 5 to 25 m deep. Rudists *Toucasia*, bivalve *Chondrodonta*, green algae, foraminifera, and numerous bioturbations (*Planolites* and *Thalassinoides*) point again to normal marine conditions. The overall succession, except for the first 160 m, where samples have been

recovered from marine episodes only, and at 280 m (corresponding to the emersion event represented by SB II-1), from which no sample has been collected, is thus deposited under normal marine conditions. Therefore, all the sampled bivalves have been recovered from levels preserved from brackish or hypersaline influences. Stenohaline assemblages like those observed in this section, such as corals, echinoderms, or large benthic foraminifera, can only tolerate salinities ranging from 30 to 40 parts per thousand (ppt) according to the literature [Kleyvas *et al.*, 1999; Benton and Harper, 2009]. Yet the diversity observed in the assemblages throughout the section suggests that salinity was likely closer to the average value of this range rather than near the limits of tolerance of these organisms [Vennin and Aurell, 2001]. In this last case anomalies in the assemblage diversity would have been expected [Lirman *et al.*, 2003; Gornitz, 2009], which is not observed in the section.

#### 4. Material and Methods

Thirty-six oysters and 19 requienids (rudists) were sampled through the Aliaga section (Figure 3) and analyzed for  $\delta^{18}\text{O}$  (Table 1). All rudist and oyster shells were carefully screened for potential diagenetic alteration using cathodoluminescence microscopy, and only the nonluminescent parts were sampled for isotope analyses (Figure 5). In order to average seasonal temperature and  $\delta^{18}\text{O}$  seawater variations, which are well expressed in organisms living in shallow environments [e.g., Steuber *et al.*, 2005], the shells were sampled using a microdrill on a length varying from 0.5 to 4 cm (on 1 to 2 cm on average) depending on the preservation of the shell, thereby crossing several growth lines. Because the trochospiral growth of requienids limits the length of shell available on a single section, it was not possible to sample rudists on a length of more than 4 cm. Because the preservation was not homogeneous within each shell, the sampling was not always realized along a continuous line. The powder was gathered into a single sample for each shell (Figure 5).

Isotope analyses were performed at the GeoZentrum Nordbayern (Erlangen, Germany). Calcite powders were reacted with 100% phosphoric acid at 75°C using a Kiel III online carbonate preparation line connected to a ThermoFinnigan 252 mass spectrometer. All isotopic values are reported in the standard  $\delta$  notation in per mil relative to VPDB (Vienna Pee Dee Belemnite) by assigning a  $\delta^{13}\text{C}$  value of +1.95‰ and a  $\delta^{18}\text{O}$  value of -2.20‰ to NBS19. Reproducibility was checked by replicate analysis of laboratory standards and was  $\pm 0.05\text{‰}$  ( $1\sigma$ ) for oxygen isotopes and  $\pm 0.02\text{‰}$  ( $1\sigma$ ) for carbon isotopes.

Eighty-three samples from the Forcall and Villarroya de los Pinares Formations of the Villarroya de los Pinares outcrop were studied for calcareous nannofossils. Simple smear slides were prepared for relative abundance count analyses [Bown and Young, 1998]. Most of the samples revealed to be barren in nannofossils, and productive samples were only recorded within the middle part of the Forcall Formation. This interval corresponds to a high sea level according to the sequence stratigraphy interpretations [Embry *et al.*, 2010; Bover-Arnal *et al.*, 2010] (sequence I-2 HST, Figure 3), and the nannofossil record may indicate that the basin was deep enough to allow the development of calcareous nannoplankton.

In the 20 productive samples, a variable number but at least 30 specimens of the 19 recorded nannoconid species were measured for length and maximum width of the nannolith and of its central canal (a total of 3320 measurements on 830 specimens). As nannoconid average length fluctuations match those of maximum width (Figure 6), only the average values of nannoconid length per sample are shown in Figure 3.

Note that absolute ages for the Barremian samples in Table 1 and in Figure 4 are only given as rough estimates, as to our knowledge no reliable biostratigraphic markers have been published that would allow datation of the Artoles Formation on the Galve platform. The absolute ages for these samples have been calculated based on Schudack and Schudack [2009], who attribute the Artoles Formation to the whole Barremian, and on the position of our samples within this formation (from 0 to 162 m at the base of the section).

#### 5. Results

##### 5.1. Oxygen Isotopes

The oxygen isotope composition of well-preserved (Figure 5) rudist and oyster shells ranges between -1 and -5‰ at Aliaga (Table 1 and Figure 3). The  $\delta^{18}\text{O}$  values of both oysters and rudists display a consequent scatter within a single stratigraphic level, of 1.5‰ on average but up to 3.3‰. Minimum  $\delta^{18}\text{O}$  values occur at the base of the section, at about 130 m, ranging from approximately -1.1‰ to approximately -4‰, and appear to decrease down to minimum values ranging from -3.9‰ to -4.9‰ at 237 m from the base

**Table 1.** Stratigraphic Position, Absolute Ages, Carbon and Oxygen Isotope Composition of the Bivalves From the Aliaga Section, and Reconstructed Paleotemperatures<sup>a</sup>

| Sample Name  | Org. | Position From the Base of the Section (m) | Absolute Ages <sup>b</sup> (Ma) | $\delta^{13}\text{C}$ (‰VPDB) | $\delta^{18}\text{O}$ (‰VPDB) | Temperature <sup>c</sup> (°C) |
|--------------|------|---|---------------------------------|-------------------------------|-------------------------------|-------------------------------|
| Al1-1H2      | O    | 131                                       | 125.96                          | -0.29                         | -3.02                         | 26.3                          |
| Al1-1H3      | O    | 131                                       | 125.96                          | 2.18                          | -1.92                         | 21.2                          |
| Al 1-2 H2-2a | O    | 133                                       | 125.90                          | -0.89                         | -3.95                         | 30.8                          |
| al1-2h2      | O    | 133                                       | 125.90                          | 0.88                          | -2.13                         | 22.2                          |
| Al 1-2 H3-2a | O    | 133                                       | 125.90                          | 0.81                          | -2.57                         | 24.2                          |
| Al1-2 H1-3   | O    | 133                                       | 125.90                          | -0.45                         | -3.23                         | 27.3                          |
| al1-3h2      | O    | 133.6                                     | 125.88                          | 0.24                          | -2.06                         | 21.9                          |
| al1-3h3      | O    | 133.6                                     | 125.88                          | 1.10                          | -1.09                         | 17.6                          |
| al1-3h       | O    | 133.6                                     | 125.88                          | 2.67                          | -1.37                         | 18.8                          |
| al1-3h1      | O    | 133.6                                     | 125.88                          | -0.48                         | -2.69                         | 24.8                          |
| Al1-8essai2  | O    | 152                                       | 125.31                          | 1.79                          | -2.72                         | 24.9                          |
| Al 1-8 H 4   | O    | 152                                       | 125.31                          | 1.94                          | -2.06                         | 21.9                          |
| Al1-8h3l1    | O    | 152                                       | 125.31                          | 1.02                          | -2.65                         | 24.6                          |
| Al1-8h3      | O    | 152                                       | 125.31                          | 2.07                          | -1.68                         | 20.2                          |
| Al1-8h1      | O    | 152                                       | 125.31                          | 1.42                          | -3.49                         | 28.6                          |
| Al1-9h1bis   | O    | 155.5                                     | 125.2                           | 0.50                          | -3.1                          | 26.7                          |
| Al1-9h4a     | O    | 155.5                                     | 125.2                           | 0.53                          | -2.88                         | 25.6                          |
| Al1-9h3bis   | O    | 155.5                                     | 125.2                           | 1.58                          | -3.4                          | 28.1                          |
| Al1-9h3      | O    | 155.5                                     | 125.2                           | 0.22                          | -3.69                         | 29.5                          |
| Al1-9h2      | O    | 155.5                                     | 125.2                           | 2.59                          | -2.13                         | 22.2                          |
| Al1-9h6      | O    | 155.5                                     | 125.2                           | 2.13                          | -2.74                         | 25                            |
| Al1-9h5      | O    | 155.5                                     | 125.2                           | 0.28                          | -2.91                         | 25.8                          |
| Al1-16r3     | O    | 187                                       | 123.3                           | 1.34                          | -3.58                         | 29                            |
| Al1-16r2     | O    | 187                                       | 123.3                           | 1.64                          | -2.48                         | 23.8                          |
| Al1-17h3     | O    | 198.1                                     | 123.1                           | 1.78                          | -4.91                         | 35.7                          |
| Al1-17h1     | O    | 198.1                                     | 123.1                           | 2.44                          | -1.74                         | 20.4                          |
| Al1-18h2     | O    | 201.8                                     | 123                             | 3.12                          | -1.47                         | 19.3                          |
| al1-18h5     | O    | 201.8                                     | 123                             | 2.14                          | -2.66                         | 24.6                          |
| Al1-18h4a    | O    | 201.8                                     | 123                             | 1.46                          | -4.21                         | 32.1                          |
| Al1-18h3     | O    | 201.8                                     | 123                             | 2.50                          | -4.45                         | 33.4                          |
| Al2-1h4      | O    | 237                                       | 122.3                           | 0.48                          | -3.91                         | 30.6                          |
| Al2-1h2      | O    | 237                                       | 122.3                           | 0.71                          | -3.98                         | 31                            |
| Al2-1h1      | O    | 237                                       | 122.3                           | 0.64                          | -4.93                         | 35.8                          |
| Al2-3a       | O    | 257.8                                     | 121.9                           | 5.02                          | -2.54                         | 24.1                          |
| Al2-3h1      | O    | 257.8                                     | 121.9                           | 4.04                          | -2.71                         | 24.8                          |
| Al2-3h3      | O    | 257.8                                     | 121.9                           | 3.22                          | -3.58                         | 29                            |
| Al2-11r4     | R    | 262.5                                     | 121.7                           | 5.76                          | -1.39                         | 18.9                          |
| Al2-11r3a    | R    | 262.5                                     | 121.7                           | 4.50                          | -2.59                         | 24.3                          |
| Al2-11r1     | R    | 262.5                                     | 121.7                           | 5.49                          | -2.2                          | 22.5                          |
| Al2-11r5     | R    | 262.5                                     | 121.7                           | 5.37                          | -2.92                         | 25.8                          |
| Al3-3h2      | O    | 285.5                                     | 119                             | 1.93                          | -2.68                         | 24.7                          |
| Al3-3h3      | O    | 285.5                                     | 119                             | 4.25                          | -2.97                         | 26.1                          |
| Al 3-3 H2b   | O    | 285.5                                     | 119                             | 4.65                          | -2.24                         | 22.7                          |
| al3-3h1a     | O    | 285.5                                     | 119                             | 2.43                          | -1.71                         | 20.3                          |
| Al3-6r1      | R    | 313.5                                     | 117                             | 4.66                          | -1.93                         | 21.3                          |
| Al3-6h1      | O    | 313.5                                     | 117                             | 2.63                          | -3.67                         | 29.4                          |
| Al3-6r3      | R    | 313.5                                     | 117                             | 4.17                          | -2.08                         | 22                            |
| Al3-6r3l2+3  | R    | 313.5                                     | 117                             | 3.94                          | -2.88                         | 25.6                          |
| Al3-6r2      | R    | 313.5                                     | 117                             | 3.80                          | -3.43                         | 28.3                          |
| Al3-7r1      | R    | 315                                       | 116.9                           | 2.99                          | -3.75                         | 29.8                          |
| Al 3-7 R2    | R    | 315                                       | 116.9                           | 2.54                          | -4.05                         | 31.3                          |
| Al3-7r3      | R    | 315                                       | 116.9                           | 3.15                          | -2.05                         | 21.8                          |
| Al3-7r5b     | R    | 315                                       | 116.9                           | 2.90                          | -3.6                          | 29.1                          |
| Al 3-10 H4   | O    | 331                                       | 115.7                           | 3.26                          | -2.7                          | 24.8                          |
| Al 3-10 H3   | O    | 331                                       | 115.7                           | 1.58                          | -2.86                         | 25.5                          |
| Al 3-10 H6   | O    | 331                                       | 115.7                           | 2.84                          | -2.58                         | 24.2                          |

<sup>a</sup>Org. = organism (O = oyster; R = rudist).

<sup>b</sup>Based on the timescale of *Ogg et al.* [2008].

<sup>c</sup>Calculated using the equation of *Anderson and Arthur* [1983] and a  $\delta^{18}\text{O}$  seawater of  $-0.7\text{‰}$  [*Zhou et al.*, 2008].

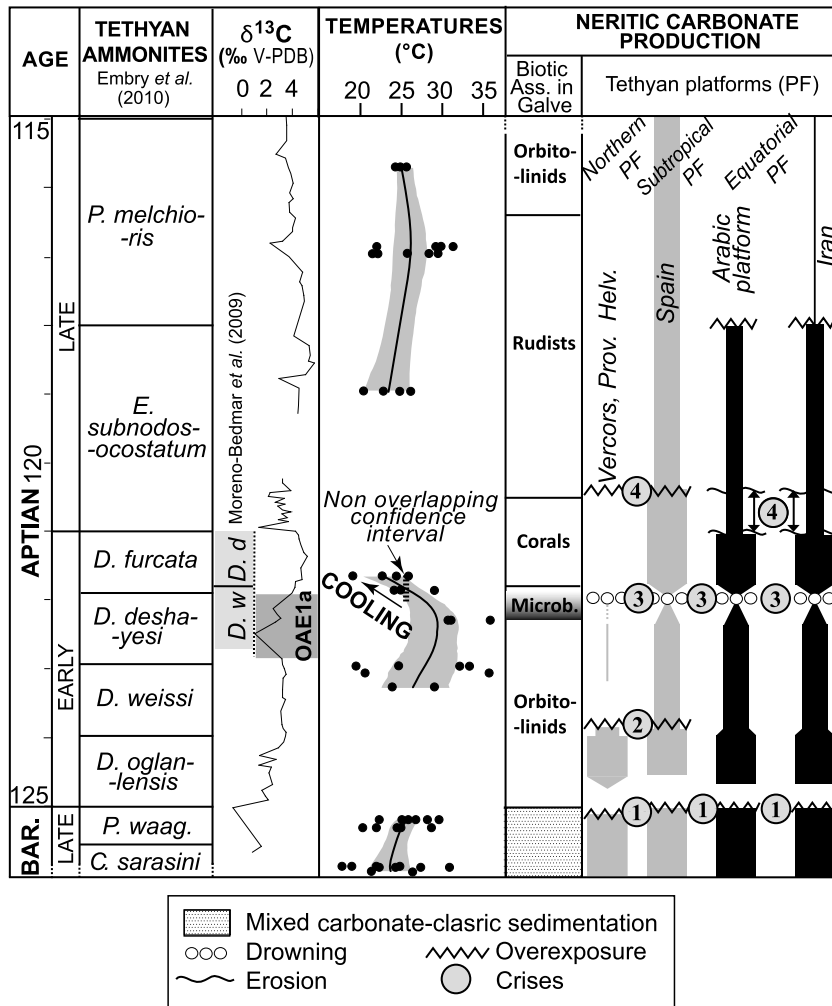


**Figure 4.** Evolution of temperatures calculated from bivalve  $\delta^{18}\text{O}$  from the Aliaga section. Temperature calculation: black curve and grey interval as in Figure 1. Absolute ages are from *Ogg et al.* [2008]. The  $\delta^{13}\text{C}$  curve has been established by analyzing micrites in the Miravete section on the Galve platform and was stratigraphically calibrated by ammonite biostratigraphy [Embry et al., 2010]. Platform neritic producers at Aliaga reported next to the temperature curve are from Embry et al. [2010]. Evolution of carbonate production on platforms is from Arnaud et al. [1998], Föllmi and Gainon [2008], and Masse [1993] for the northern Tethys; Embry et al. [2010] for Spain (subtropical platform); and van Buchem et al. [2010] for equatorial platforms (Arabia and Oman). (second column) The Tethyan ammonite biozones follow the interpretation of Embry et al. [2010]. However, because the local position of Aptian ammonite biozones is still discussed in the Maestrat Basin, the existing alternative interpretation is also presented in grey on the figure [Moreno-Bedmar et al., 2009]. BAR. = Barremian, P. waag. = *P. Waagenoides*, D.w = *D. weissii* ammonite zone, and D. d = *D. deshayesi* ammonite zone according to the alternative interpretation of Moreno-Bedmar et al. [2009]. Microb. = microbialites and Biotic Ass. In Galve: biotic assemblages in Galve. (fifth column) The numbers are attributed to the different platform crises that are discussed in the text.

of the section. A marked increase in bivalve  $\delta^{18}\text{O}$  values is then recorded up to maximum values in the  $-1.4$  to  $-2.9\text{‰}$  range at 262.5 m from the base of the section. Oxygen isotope values recorded by the rudists then remain in the  $-1.7$  to  $-4\text{‰}$  range for the remaining of the section.

**5.2. Calcareous Nannofossils**

Calcareous nannofossils were recorded in only 22 of the 83 studied samples. The lowest sample bearing a few nannoconids but not coccoliths was recorded at ~212 m. Above that, samples were completely barren in nannofossils until 255 m. In general, the samples contain a diversified nannoconid assemblage (19 different species were observed in all the studied interval; Figure 6), while coccolith assemblage is low diversified and mainly represented by large-sized specimens of *Watznaueria barnesiae*, *W. manivitia*, *Zeughrabdotos embergeri*, *Cretarhabdus* spp., and *Rhagodiscus asper*. Pentaliths (mainly *Micrantholithus obtusus*) are only

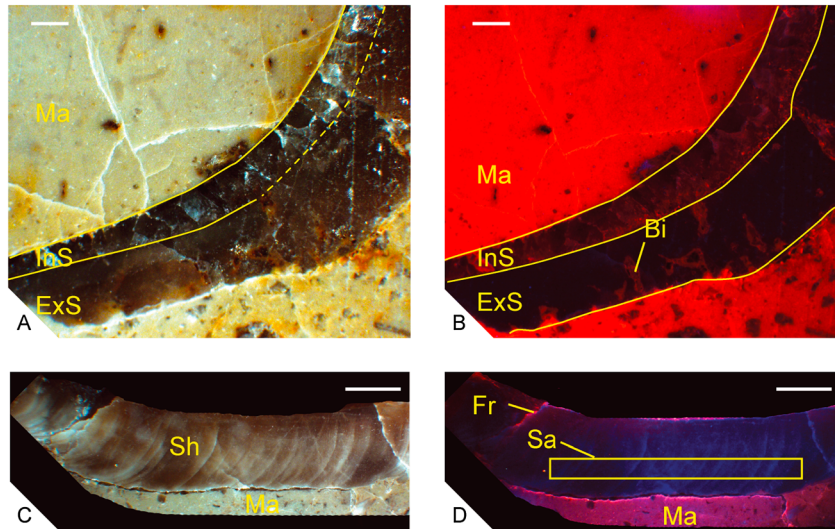


**Figure 5.** Preservation and sampling of bivalve shells. (a and b) Scale bar = 500  $\mu\text{m}$  and (c and d) scale bar = 2000  $\mu\text{m}$ . Rudist shell enclosed in a packstone matrix (Ma) observed in natural light displaying its intrashell (InS) recrystallized in high magnesium calcite and its external shell (ExS) (Figure 5a). Rudist shell A observed under cathodoluminescence allowing to distinguish bioerosion (Bi) which affect the rudist shell (Figure 5b). Rudist shell (Sh.) VP6-10 observed in natural light, enclosed in a packstone matrix (Ma) (Figure 5c). Rudist shell C observed under cathodoluminescence displaying luminescent calcite in a fracture (Fr) and a large nonluminescent area that corresponds to a well-preserved calcite sampled for isotope analysis (Sa = sampled area) (Figure 5d).

recorded in the interval between 280 and 290 m. The nannolith *Assipetra* is sporadically recorded. Overall preservation of coccoliths is poor with overgrowth being more important than etching. Diagenesis may explain the low recorded diversity. As nannoconids are common in most of the productive samples and better preserved than coccoliths, size measurements were done on the nannoconids.

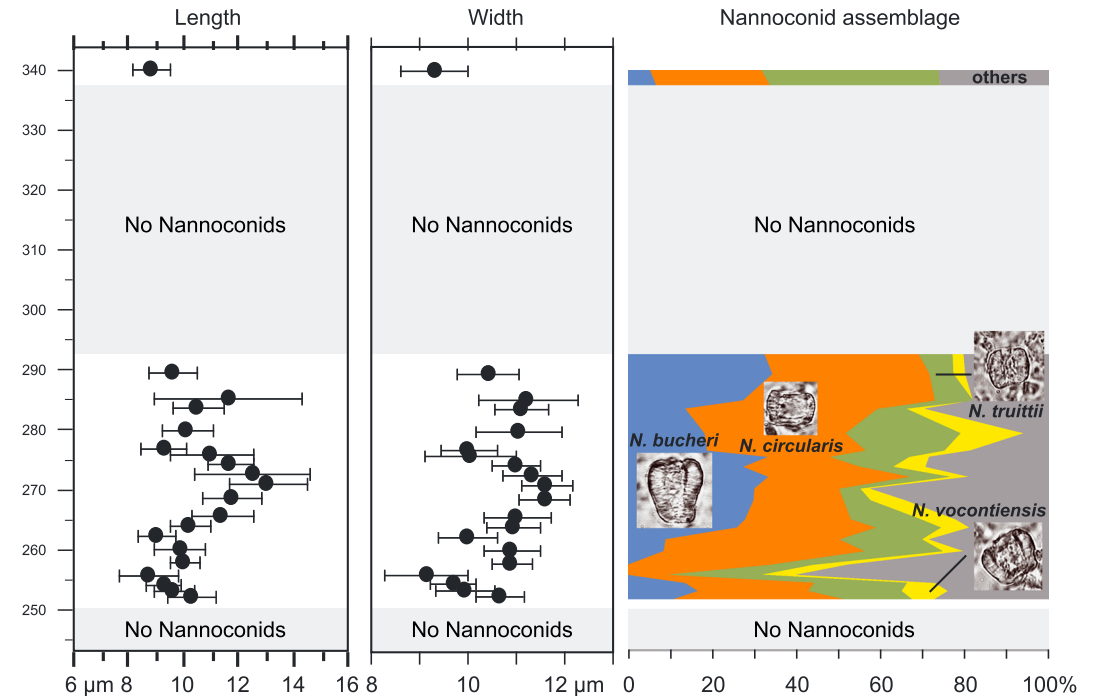


**Figure 6.** Average length and width of *Nannoconus* in the studied samples. Error bar = 95% confidence interval. Proportions of various *Nannoconus* species in the total nannoconid pool as measured in the studied samples. The change in dominant species likely accounts for a part of the observed size increase during the cooling period.

**Table 2.** Average Values of Nannoconid Length, Width, and Central Canal Length and Width

| Villaroya | Sample | Position on the Section (m) | Average Nannoconid |            |                |               |
|-----------|--------|-----------------------------|--------------------|------------|----------------|---------------|
|           |        |                             | Length (μm)        | Width (μm) | CA Length (μm) | CA Width (μm) |
| VI 09     | 23     | 252.00                      | 10.32              | 10.68      | 6.10           | 4.47          |
| VI 09     | 25     | 253.00                      | 9.69               | 9.94       | 5.72           | 3.92          |
| VI 09     | 29     | 254.50                      | 9.30               | 9.70       | 5.45           | 3.82          |
| VI 09     | 30     | 255.20                      | 8.77               | 9.15       | 5.67           | 3.22          |
| VI 09     | 31     | 257.40                      | 10.07              | 10.91      | 6.69           | 4.85          |
| VI 09     | 33     | 260.00                      | 9.90               | 10.90      | 6.44           | 5.19          |
| VI 09     | 35     | 262.50                      | 9.03               | 10.00      | 5.41           | 4.44          |
| VI 09     | 38     | 264.00                      | 10.27              | 10.94      | 6.64           | 4.78          |
| VI 09     | 40     | 265.50                      | 11.42              | 11.02      | 7.46           | 4.45          |
| VI 09     | 42     | 268.50                      | 11.79              | 11.58      | 8.15           | 4.66          |
| VI 09     | 45     | 270.50                      | 13.08              | 11.64      | 8.54           | 4.51          |
| VI 09     | 48     | 272.50                      | 12.51              | 11.32      | 8.52           | 4.66          |
| VI 09     | 50     | 274.50                      | 11.70              | 10.99      | 8.29           | 5.37          |
| VI 09     | 53     | 275.50                      | 11.04              | 10.06      | 6.76           | 3.90          |
| VI 09     | 55     | 277.00                      | 9.33               | 10.03      | 6.26           | 4.55          |
| VI 09     | 56     | 280.00                      | 10.14              | 11.05      | 6.51           | 5.01          |
| VI 09     | 59     | 283.00                      | 10.55              | 11.11      | 7.23           | 5.02          |
| VI 09     | 60     | 285.00                      | 11.64              | 11.23      | 7.61           | 4.42          |
| VI 09     | 63     | 289.50                      | 9.60               | 10.42      | 5.82           | 4.22          |
| VI 09     | 83     | 340.00                      | 8.90               | 9.31       | 5.15           | 2.47          |

Nannoconid length seems to be a good descriptor of changes in size through time. At Villaroya de Los Pinares, our data show significant variations in nannoconid average size within the studied interval. Small nannoconid sizes are recorded, from 10.3 μm to 8.7 μm, at the top of the Forcall Formation between 250 and 260 m, which corresponds to the latest part of the interval equivalent to OAE1a in this section (C5, C6, and part of C7 isotopic segments) [Menegatti et al., 1998; Embry et al., 2010]. These small sizes are followed by an important nannoconid size increase up to maximum average values of 13 μm in the interval that correlates with the maximum δ<sup>18</sup>O values recorded in the bivalves at Aliaga, from 260 to about 270 m from the base of the section. The data may then present a decrease to pre-excursion size values, but the error bars overlap (Figure 3). Nannoconid width average sizes follow the same patterns as length (Figure 6). The size variations observed in nannoconids also correspond to a change in the dominance in the nannoconid assemblage, with the largest length observed corresponding to a dominance of *N. bucheri* (Figure 6). Size changes thus correspond to both assemblage composition and species-specific size fluctuations. By contrast, all the studied samples present large central canal widths comprised between 4 and 5.5 μm (Table 2), indicating that mostly wide-canal nannoconids occurred during the studied interval. Such an occurrence of wide-canal nannoliths after OAE1a was already described in the literature [Erba, 1994; Erba and Tremolada, 2004].

## 6. Discussion

### 6.1. Paleotemperature Record of the Aliaga Platform

No vital fractionation effects have been described so far for oysters and *Requiniidae* [Surge et al., 2001; Steuber et al., 2005], as it is the case for most bivalve species and fossil rudists [Wefer and Berger, 1991; Steuber, 1996, 1999; Lécuyer et al., 2004; Ullmann et al., 2010; Shöne and Gillikin, 2013]. The absence of ( $R^2 = 0.0754$ ) or weak ( $R^2 = 0.5059$ ) correlation between δ<sup>18</sup>O and δ<sup>13</sup>C values in the oyster and rudist data sets, respectively, supports this view (Figure 7) [McConnaughey, 1989a, 1989b; Auclair et al., 2003; Parkinson et al., 2005]. Although vital effects cannot be completely excluded, the weak correlation observed in our rudist isotopic data could arise from covariations in temperature and local dissolved inorganic carbon δ<sup>13</sup>C, as can be observed in modern and fossil bivalves [e.g., Steuber, 1996; Kirby et al., 1998; Surge et al., 2003]. We therefore compiled the δ<sup>18</sup>O values of both taxa into a single data set and applied the equation of Anderson and Arthur [1983] for paleotemperature calculations. We used a δ<sup>18</sup>O value of −0.7‰ for Cretaceous seawater as modeled by Zhou et al. [2008], accounting for the absence of continental ice sheets and local effects of evaporation, precipitation, and runoff.

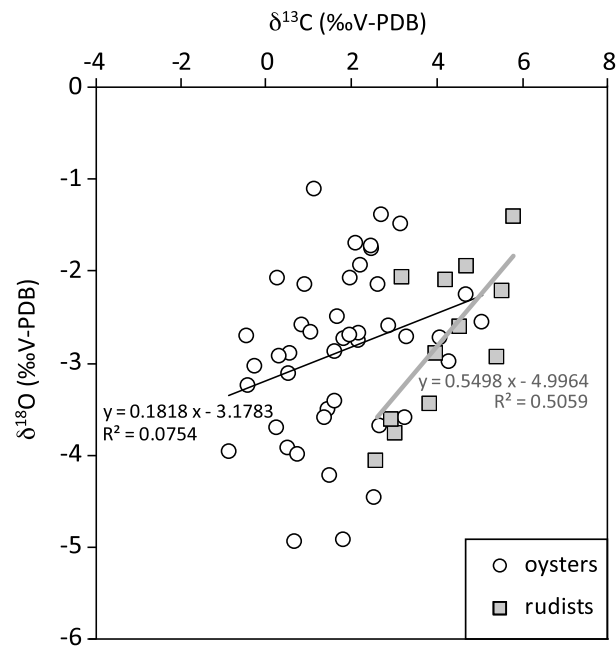


**Figure 7.** Oxygen versus carbon isotope composition of the oysters (open circles) and rudists (grey squares) analyzed at Aliaga. The linear regression has been conducted on rudist and oyster data altogether.

For individual studied levels, a large scatter in  $\delta^{18}\text{O}$  values of 1.5‰ on average with a maximum variation of 3.3‰ is observed (Figure 3). This range is comparable to or slightly lower than the  $\delta^{18}\text{O}$  range observed in individual Cretaceous rudist shells by Steuber *et al.* [2005]. Similarly to Steuber *et al.* [2005], this relatively large range is likely here to result as well from seasonal variations in temperature and  $\delta^{18}\text{O}$  of seawater, which are both well expressed in shallow open marine environments. The largest dispersion is observed in the intervals displaying the shallowest conditions (from the base of the section to 205 m and above 280 m). Although no anomaly in the diversity of the stenohaline assemblages is observed during these intervals, these assemblages may accommodate larger salinity variations on short (seasonal) time-scales. This large dispersion indicates that only a small part of the intrashell variation in  $\delta^{18}\text{O}$  has thus been averaged by our sampling method, which gathered calcite on

individual shells on an average length of 1 to 2 cm only. Indeed, although several growth lines were crossed when sampling each shell, each growth increment in bivalves does not necessarily represent an annual cycle but may represent shorter intervals [e.g., Schöne *et al.*, 2004; Steuber *et al.*, 2005, Supplementary Material; Ullmann *et al.*, 2010, 2013].

Because of the large scatter in  $\delta^{18}\text{O}$ , we applied statistical methods to determine whether significant trends in bivalve  $\delta^{18}\text{O}$  evolution can be identified. We first adjusted a kernel regression curve [e.g., Ruppert *et al.*, 2003] to the data set and computed a 95% confidence interval (grey area; Figure 3) from 1000 bootstrapped samples, using the function “locally.weighted.polynomial” from the “SiZer” package in R ([www.r-project.org](http://www.r-project.org)). Along the adjusted Kernel curve, the nonoverlapping 95% confidence interval indicates a significant trend. At Aliaga, a decrease of over 1‰ on average in bivalve  $\delta^{18}\text{O}$  values may have occurred during the Early Aptian with minimum values recorded during the OAE1a. Yet since the confidence intervals overlap during this interval, this trend is not considered as statistically significant. If further confirmed, part of this possible decrease in bivalve  $\delta^{18}\text{O}$  values may reflect a limited decrease in salinity, although within the range of tolerance of the stenohaline assemblages observed on the platform (see section 3). Environments become deeper and more open to the rest of the basin as they evolve from lower shoreface to the deep offshore. If solely due to temperature, this decrease would translate into a 5°C warming at Aliaga. Such a warming would be supported by the existence of cooler conditions at the base of the Aptian as highlighted by Tethyan fish tooth and rudist  $\delta^{18}\text{O}$  data [Pucéat *et al.*, 2003; Steuber *et al.*, 2005] and subsequent warmer conditions within OAE1a inferred from equatorial Pacific TEX86 data [Dumitrescu *et al.*, 2006]. These TEX86 data point to temperatures ranging from 30 to 36°C, which are similar to temperatures inferred from oyster  $\delta^{18}\text{O}$  at Aliaga for the interval equivalent to OAE1a (30–35°C, Figure 3). A warming trend prior to and at the base of OAE1a has also been suggested based on evolution of sporomorph assemblages, showing an increase in *Classopollis* and *Araucariacites* spp. along with a decrease in bisaccate pollen percentages, and bulk rock  $\delta^{18}\text{O}$  from the north of Italy and from central Pacific Ocean [Keller *et al.*, 2011; Ando *et al.*, 2008].

A statistically significant (nonoverlapping confidence intervals) increase of over 1‰ on average in bivalve  $\delta^{18}\text{O}$  values is then recorded during the late Early Aptian. It would translate into a 5°C cooling if solely due to a change in sea surface temperatures. The onset of this increase that occurs within the interval of nonoverlapping confidence intervals (Figures 3 and 4) postdates most of OAE1a. Increase in phosphorus concentrations and in inputs of siliciclastics within OAE1a at Galve and in the Umbria-Marche Basin [Embry *et al.*, 2010; Stein *et al.*, 2011] hints

toward more humid conditions in this basin prior to and during OAE1a. The replacement of mesotrophic (orbitolinids, bivalves, and microbialites) by oligotrophic organisms (coral and stromatoporoid reefs) just after MFS I-2, during the increase in bivalve  $\delta^{18}\text{O}$  values, suggests a reduction in nutrient inputs in the region of Aliaga after OAE1a. Nutrients could be brought on continental shelves by the arrival of deeper, cooler, and nutrient-rich water through upwelling processes like on the Helvetic platform where the occurrence of highly condensed and phosphate-rich beds follows the platform demise observed prior to or during OAE1a [Föllmi *et al.*, 2006; Föllmi and Gainon, 2008]. Yet there is no such evidence for the occurrence of upwelling at Aliaga during the intervals characterized by mesotrophic biotic assemblages. The change in trophic levels suggested by the evolution from mesotrophic to oligotrophic organisms is to our opinion more likely here to reflect changes in the hydrological regime, from a more humid to a drier climate.

In that case, we cannot exclude that part of the recorded increase in bivalve  $\delta^{18}\text{O}$  could derive from an increase in the evaporation-precipitation budget. The change in seawater  $\delta^{18}\text{O}$  of over 1‰ that would be required to explain the bivalve  $\delta^{18}\text{O}$  signal entirely in terms of changes in seawater  $\delta^{18}\text{O}$  would correspond to a salinity change of over 10 ppt, according to existing salinity- $\delta^{18}\text{O}_{\text{seawater}}$  relationships established in similar low-latitude environments [Fairbanks *et al.*, 1992]. The interval defining the  $\delta^{18}\text{O}$  increase corresponds to stenohaline biotic assemblages, evolving from foraminifers (orbitolinids), ammonite fragments, echinoderms, and bivalves *Trigonia* sp. and *Neithea* sp. assemblages in a storm-induced upper offshore environment to *Bacinnella*, foraminifers, corals, stromatoporoids, echinoderms, and serpulids assemblages in a transitional offshore to lower shoreface environment (Figure 2; see section 3 for further details). A 10 ppt change in salinity would encompass the entire range of tolerance of these organisms, from 30 to 40 ppt [Kleypas *et al.*, 1999; Benton and Harper, 2009]. Yet throughout all this interval, no anomaly in the fossil record diversity is observed, as it would be expected if salinity reached the limit of tolerance of these stenohaline assemblages [Vennin and Aurell, 2001; Lirman *et al.*, 2003; Gornitz, 2009]. On the opposite, the diverse biotic assemblages observed during this interval point to quite stable salinity conditions. In addition, this increase in bivalve  $\delta^{18}\text{O}$  values occurs during an interval of high sea level, close to MFS I-2 that records the deepest conditions on the platform, at approximately 40 m. Changes in the evaporation minus precipitation budget should therefore have the lowest impact on the local marine environments during this interval. For these reasons, we consider that salinity changes unlikely drove the recorded  $\delta^{18}\text{O}$  increase. This trend is thereafter interpreted as a decrease of seawater temperature on the Aliaga platform.

Our data within OAE1a are too scarce to allow direct comparison with existing high-resolution bulk carbonate  $\delta^{18}\text{O}$  records. Yet it could be noted that a cooling trend has been recognized based on bulk rock  $\delta^{18}\text{O}$ , beginning within OAE1a and with variable duration according to authors, both in the Tethys and in the Pacific [Hochuli *et al.*, 1999; Ando *et al.*, 2008; Kuhnt *et al.*, 2011]. Changes in sporomorph assemblages, with a rise in bisaccate pollen after OAE1a, have been interpreted to reflect a cooling episode as well [Hochuli *et al.*, 1999], although this interpretation has been discussed [Heimhofer *et al.*, 2004; Keller *et al.*, 2011]. Moreover, hinterland vegetation changes have been evidenced in the western Maestrat Basin and related to a pronounced cooling during the late Early Aptian [Cors *et al.*, 2013; Bover-Arnal *et al.*, 2014].

## 6.2. Links Between Climate and Carbonate Production

The bivalve  $\delta^{18}\text{O}$  record from the Aliaga platform allows us for the first time to compare at the same site the evolution of sea surface temperatures with the evolution of neritic carbonate producers on the platform and of pelagic carbonate producers (i.e., nannofossils). Up to the temperature maximum in the late Early Aptian (upper part of the Forcall Formation), carbonate production is dominated by orbitolinids. The platform demise observed in the northern Tethyan domain in the earliest Aptian (crisis 2, Figure 3) [Arnaud *et al.*, 1998; Föllmi and Gainon, 2008; Godet, 2013] corresponds to a sequence boundary (SBI-2, Figure 4) interpreted to represent a relative sea level fall [Embry *et al.*, 2010]. SBI-2 is not marked by any major change in the association of carbonate producers. This carbonate platform demise has been attributed to a short-term regression, probably tectonically driven, interrupting a long-term rise in relative sea level [Embry *et al.*, 2010]. After crisis 2, expressed by SBI-2, the carbonate production does not fully recover but remains lower than before crisis 2. Following this limited recovery, an increase in clay content is observed on the Aliaga platform [Embry *et al.*, 2010] (Figure 3), as on other southern Tethyan platforms (Oman, Qatar, Saudi Arabia, and UAE) [van Buchem *et al.*, 2010]. The climax of this subsequent carbonate production demise coincides with crisis 3 expressed by the MFS I-2 (Figure 4). This succession of crises recorded during the

Early Aptian on the Aliaga platform follows the trend of latitudinal restriction of rudist-rich platforms described by *Skelton and Gili* [2012], culminating during OAE1a in association with a dominance of microbial carbonates. The interval from SBI-2 up to MFS I-2 is contemporaneous to an absence of carbonate production on the northern Tethyan platforms (Helvetic, Provence, and Vercors), as expressed by condensed levels (Figure 4) [Masse, 1993; Arnaud *et al.*, 1998; Föllmi and Gainon, 2008]. The temperature maximum documented by bivalve  $\delta^{18}\text{O}$  values from the Aliaga platform coincides with OAE1a interval in basins (Figure 4), which is associated to a positive  $\delta^{13}\text{C}$  excursion, and corresponds to the Aliaga platform and on the southern Tethyan platforms to the development of microbialites (Figure 4) [e.g., Embry *et al.*, 2010; Huck *et al.*, 2011; Bover-Arnal *et al.*, 2010]. Also, a nannoconid crisis, corresponding to an interval completely devoid of representatives of the genus *Nannoconus*, is recognized in Tethyan basins during OAE1a [Erba and Tremolada, 2004]. In Villarroya de los Pinares, evidence of this crisis may be expressed by the low nannoconid size measured in the upper part of OAE1a time equivalent.

Enhanced nutrient delivery to the oceans during OAE1a, maybe favored by the high temperatures illustrated by the bivalve  $\delta^{18}\text{O}$  that could have driven an intensification of chemical weathering, has been suggested based on an increase in phosphorus concentrations and enhanced inputs of siliciclastics within OAE1a at Galve and in the Umbria-Marche Basin during the time interval of OAE1a [Embry *et al.*, 2010; Stein *et al.*, 2011]. More specifically, microbialite development follows enhanced siliciclastic input recorded in the Aliaga platform (Figures 2 and 3). Mesotrophic conditions may therefore have favored the development of microbialites during this interval [e.g., Huck *et al.*, 2011, 2012]. The decrease in marine temperatures recorded at Aliaga is concomitant to a major change in biotic associations, characterized by the development of corals, the occurrence of nannoconids, as well as an important increase in nannoconid size documented at Villarroya de los Pinares (from 8.7 to 13  $\mu\text{m}$ ; Figures 3 and 6). At Aliaga, it has been suggested that this evolution from heterozoan (microbialites) to photozoan (corals) organisms may have been driven by a change from humid toward drier climate conditions [Embry *et al.*, 2010]. Such a change could have been favored by the cooler climatic conditions recorded by the bivalve isotopic composition analyzed in this work. The major role of trophic levels in the evolution of platform carbonate producers has been already emphasized in several studies [Föllmi *et al.*, 1994; Weissert *et al.*, 1998; Föllmi *et al.*, 2006], and our work supports this view.

An evolution toward oligotrophic conditions in surface waters may also have driven the observed increase in nannoconid abundance, as these nannoliths are interpreted as deep dwellers, proliferating when nutricline settles deep in the photic zone [Erba, 1994, 2004], while size changes are more difficult to interpret. Interestingly, a nannoconid increase both in abundance and size has also been reported by Barbarin *et al.* [2012] in the Vocontian Basin during cool marine conditions in the mid-Valanginian, concomitant with the maximum of the  $\delta^{13}\text{C}$  positive excursion of the Weissert event [Bralower *et al.*, 1994; Erba and Tremolada, 2004; Erba *et al.*, 2004; Gréselle *et al.*, 2011; Bonin *et al.*, 2012]. This mid-Valanginian temporary recovery in nannoconid carbonate production coincides with a crisis of carbonate platforms, which may have contributed to increase  $\text{Ca}^{2+}$  and  $\text{HCO}_3^-$  concentrations in ocean waters as these ions become less involved in neritic carbonate production, favoring pelagic production [Barbarin *et al.*, 2012]. Yet the mid-Valanginian nannoconid recovery also coincides with a decrease in detrital inputs and in the proportion of kaolinite in the Vocontian Basin [Gréselle *et al.*, 2011; Barbarin *et al.*, 2012; Bonin *et al.*, 2012], suggesting a decrease in continent-derived nutrients and in water turbidity. Here the recorded nannoconid recovery may thus also be linked to a decrease in trophic levels as previously interpreted by various authors [Erba, 1994; Herrle, 2002; Erba and Tremolada, 2004; Erba *et al.*, 2004; Bornemann *et al.*, 2005]. It is interesting to note that for both periods, the recovery occurs at a time of decreased detrital inputs, confirming the important influence of low trophic levels in surface waters for the development of nannoconids. Erba [2004] inferred that carbonate production by nannoconids resumed after the excess  $\text{CO}_2$  during OAE1a disappeared. As the identified cooling culminates just after OAE1a, lower  $\text{CO}_2$  levels may also have contributed to the increase in nannoconid abundance and size observed at Villarroya de los Pinares.

Importantly, the cooling phase postdates (i) most of OAE1a (Figure 3) and (ii) the major platform demise in the northern Tethys (crisis 2, Figure 4) and the associated decrease in carbonate production on the southern margin of the Tethys, which is marked by an increase in marl contents culminating at the MFS I-2 in association with the development of microbialites at Aliaga (corresponding to crisis 3, Figure 4). As a result, the cooling cannot be responsible for the worldwide carbonate platform demise. Sequestration of atmospheric carbon during black shale deposition has been repeatedly proposed to explain intermittent cooling episodes

associated to OAEs [Kump and Arthur, 1999; Dumitrescu et al., 2006; Forster et al., 2007]. As the cooling episode recorded here begins within OAE1a, drawdown of atmospheric CO<sub>2</sub> associated to enhanced organic carbon burial represents a possible trigger mechanism for this cold snap. An alternative mechanism could be directly linked to the carbonate production crises. Indeed, numerical experiments have shown that a demise of middle-latitude carbonate platforms accompanied by a reduction of neritic carbonate production at low latitudes has the potential to generate a rapid decrease in CO<sub>2</sub> levels and short-lived cold interludes [Donnadieu et al., 2011]. Therefore, the major platform demise recorded in the northern Tethys (crisis 2) associated to the decrease in neritic carbonate production on the southern margin of the Tethys culminating at MFS 1–2 (crisis 3) could have triggered as well the cooling episode depicted in our study in the earliest Late Aptian.

## 7. Conclusions

The bivalve δ<sup>18</sup>O data presented in this study document a decrease in surface (<100 m) water temperatures of 3.8 to 5°C that postdates most of OAE1a and the worldwide carbonate platform demise recorded during the late Early Aptian. This study strongly suggests that the climate cooling cannot have triggered the demise of carbonate production on Tethyan platforms in the lower part of the Early Aptian. Conversely, both enhanced organic carbon burial and the collapse in platform carbonate production occurring in the late Early Aptian may have been responsible for a drawdown of atmospheric CO<sub>2</sub> triggering cooler climatic conditions.

The late Early Aptian cooling event is time equivalent to a major change from microbialites to coral assemblages at Aliaga. This change may result from the cooler conditions that may have favored the establishment of drier conditions at least regionally, thereby reducing the nutrient inputs brought to the oceans by continental erosion.

Finally, for the first time, nannofossil record was directly compared to platform evolution during the Aptian thanks to the exceptional record of the Galve Basin. Small nannoconid sizes are recorded during the OAE1a, which likely signs the well-known Aptian nannoconid crisis. Subsequently, a recovery in pelagic carbonate production is attested by a significant size increase of this major carbonate producer that may be linked to the cooling event through an increased aridity and decreased continental-derived nutrient inputs. Although further studies have to be conducted, the synchronous recovery of pelagic carbonate production after the OAE1a and the establishment of a coral-dominated platform may be linked to a change in the trophic levels of the surface waters.

## Acknowledgments

This work was funded by a FABER program from the Region de Bourgogne. Supporting data are included in Tables 1 and 2. Any additional data may be obtained from E.P. (e-mail: emmanuelle.puceat@u-bourgogne.fr).

## References

- Anderson, T. F., and M. A. Arthur (1983), Stable isotopes of oxygen and carbon and their application to sedimentologic and paleoenvironmental problems, in *Stable Isotopes in Sedimentary Geology*, edited by M. A. Arthur et al., pp. 1–151, Soc. of Econ. Paleontol. and Mineral., Tulsa, Okla.
- Ando, A., K. Kaiho, H. Kawahata, and T. Kakegawa (2008), Timing and magnitude of early Aptian extreme warming: Unraveling primary δ<sup>18</sup>O variation in indurated pelagic carbonates at Deep Sea Drilling Project Site 463, central Pacific Ocean, *Palaeogeogr. Palaeoclimatol. Palaeoecol.*, **260**, 463–476.
- Arnaud, H., et al. (1998), Répartition stratigraphique des orbitolinidés de la plate-forme urgonienne subalpine et jurassienne (SE de la France), *Geol. Alp.*, **74**, 3–89.
- Auclair, A.-C., M. M. Joachimski, and C. Lécuyer (2003), Deciphering kinetic, metabolic and environmental controls on stable isotope fractionations between seawater and the shell of *Terebratalia transversa* (Brachiopoda), *Chem. Geol.*, **202**, 59–78.
- Barbarin, N., A. Bonin, E. Mattioli, E. Pucéat, H. Cappetta, B. Gréselle, B. Pittet, E. Vennin, and M. Joachimski (2012), Evidence for a complex Valanginian nannoconid decline in the Vocontian basin (South East France), *Mar. Micropaleontol.*, **84–85**, 37–53, doi:10.1016/j.marmicro.2011.11.005.
- Benton, M., and D. A. T. Harper (2009), *Introduction to Paleobiology and the Fossil Record*, 608 pp., Wiley-Blackwell, Chichester, U. K.
- Bonin, A., E. Vennin, E. Pucéat, M. Guiraud, A. Arnaud, T. Adatte, B. Pittet, and E. Mattioli (2012), Community replacement in neritic carbonate organisms during the late Valanginian platform demise: A new preserved record in the Provence Platform, *Palaeogeogr. Palaeoclimatol. Palaeoecol.*, **365–366**, 57–80.
- Bornemann, A., J. Pross, K. Reichelt, J. Herrle, C. Hemleben, and J. Mutterlose (2005), Reconstruction of short-term palaeoceanographic changes during the formation of the Late Albian Niveau Breistroffer black shales (Oceanic Anoxic Event 1d, SE France), *J. Geol. Soc. London*, **162**, 623–639, doi:10.1144/0016-764903-171.
- Bover-Arnal, T., J. A. Moreno-Bedmar, R. Salas, P. Skelton, K. Bitzer, and E. Gili (2010), Sedimentary evolution of an Aptian syn-rift carbonate system (Maestrat Basin, E Spain) effects of accommodation and environmental change, *Geol. Acta: Int. Earth Sci. J.*, **8**, 249–280.
- Bover-Arnal, T., R. Salas, J. Guimera, and J. A. Moreno-Bedmar (2014), Deep incision in an Aptian carbonate succession indicates major sea-level fall in the Cretaceous, *Sedimentology*, **61**, 1558–1593.
- Bown, P. R., and J. R. Young (1998), Techniques, in *Calcareous Nannoplankton Biostratigraphy*, edited by P. R. Bown, pp. 16–28, British Micropaleontological Society, Publications Series, London, Chapman and Hall.

- Bralower, T. J., M. A. Arthur, R. M. Leckie, W. V. Sliter, D. Allard, and S. O. Schlanger (1994), Timing and paleoceanography of oceanic dysoxia/anoxia in the Late Barremian to Early Aptian, *Palaios*, *9*, 335–369.
- Canérot, J., P. Cugny, M. Garcia-Hernandez, A. C. Lopez-Garrido, B. Peybernes, J. Rey, and J. A. Vera (1982), Les principaux événements sur diverses plates-formes éocènes des bordures mésogéenne et Atlantique de la Péninsule Ibérique, *Cuad. Geol. Iber.*, *8*, 831–845.
- Cors, J., U. Heimhofer, T. Bover-Arnal, and R. Salas (2013), Spore-pollen assemblage records delayed terrestrial cooling in response to organic carbon burial during OAE1a, *Geophysical Research Abstracts* *15*, EGU 2013, 1898.
- Donnadieu, Y., G. Dromart, Y. Goddérès, E. Pucéat, B. Brigaud, G. Dera, C. Dumas, and N. Olivier (2011), A mechanism for brief glacial episodes in the Mesozoic greenhouse, *Paleoceanography*, *26*, PA3212, doi:10.1029/2010PA002100.
- Dudley, W. C., P. L. Blackwelder, L. E. Brand, and J. C. Duplessy (1986), Stable isotope composition of coccoliths, *Mar. Micropaleontol.*, *10*, 1–8.
- Dumitrescu, M., S. C. Brassell, S. Schouten, E. C. Hopmans, and J. S. S. Damste (2006), Instability in tropical Pacific sea-surface temperatures during the early Aptian, *Geology*, *34*, 833–836.
- Embry, J. C., E. Vennin, F. S. P. van Buchem, R. Schroeder, C. Pierre, and M. Aurell (2010), Sequence stratigraphy and carbon isotope stratigraphy of an Aptian mixed carbonate-siliciclastic platform to basin transition (Galve sub-basin, NE Spain), in *Mesozoic and Cenozoic Carbonate Systems of the Mediterranean and the Middle East: Stratigraphic and Diagenetic Reference Models*, edited by F. S. P. Van Buchem, K. D. Gerdes, and M. Esteban, *Geol. Soc. London, Spec. Publ.*, *329*, pp. 113–143.
- Erba, E. (1994), Nannofossils and superplumes: The early Aptian “nannoconid crisis”, *Paleoceanography*, *9*, 483–501.
- Erba, E. (2004), Clacareous nannofossils and Mesozoic anoxic events, *Mar. Micropaleontol.*, *52*, 85–106.
- Erba, E., and F. Tremolada (2004), Nannofossil carbonate fluxes during the Early Cretaceous: Phytoplankton response to nitrification episodes, atmospheric CO<sub>2</sub>, and anoxia, *Paleoceanography*, *19*, PA1008, doi:10.1029/2003PA000884.
- Erba, E., A. Bertolini, and R. G. Larson (2004), Valanginian Weissert oceanic anoxic event, *Geology*, *32*, 49–152, doi:10.1130/G20008.1.
- Fairbanks, R. G., C. D. Charles, and J. D. Wright (1992), Origin of global meltwater pulses, in *Four Decades of Radiocarbon: An Interdisciplinary Approach*, edited by A. Long, and R. Kra, pp. 473–500, Springer, New York.
- Föllmi, K. B., and F. Gainon (2008), Demise of the northern Tethyan Urgonian carbonate platform and subsequent transition towards pelagic conditions: The sedimentary record of the Col de la Plaine Morte area, central Switzerland, *Sediment. Geol.*, *205*, 142–159.
- Föllmi, K. B., H. Weissert, M. Bisping, and H. Funk (1994), Phosphogenesis, carbon-isotope stratigraphy and carbonate platform evolution along the northern Tethyan margin, *Geol. Soc. Am. Bull.*, *106*, 729–746.
- Föllmi, K. B., A. Godet, S. Bodin, and P. Linder (2006), Interactions between environmental change and shallow water carbonate buildup along the northern Tethyan margin and their impact on the Early Cretaceous carbon isotope record, *Paleoceanography*, *21*, PA4211, doi:10.1029/2006PA001313.
- Forster, A., S. Schouten, K. Moriya, P. A. Wilson, and J. S. Sinninghe Damsté (2007), Tropical warming and intermittent cooling during the Cenomanian/Turonian oceanic anoxic event 2: Sea surface temperature records from the equatorial Atlantic, *Paleoceanography*, *22*, PA1219, doi:10.1029/2006PA001349.
- Godet, A. (2013), Drowning unconformities: Palaeoenvironmental significance and involvement of global processes, *Sediment. Geol.*, *293*, 45–66.
- Gornitz, V. (2009), *Encyclopedia of Paleoclimatology and Ancient Environments, Encyclopedia of Earth Sciences Series XXVIII*, Springer, Dordrecht.
- Gréselle, B., B. Pittet, E. Mattioli, M. Joachimski, N. Barbarin, L. Riquier, S. Reboulet, and E. Pucéat (2011), The Valanginian isotope event: A complex suite of palaeoenvironmental perturbations, *Palaeoogeogr. Palaoclimatol. Palaeoecol.*, *306*, 41–57.
- Heimhofer, U., P. A. Hochuli, J. O. Herrle, N. Andersen, and H. Weissert (2004), Absence of major vegetation and palaeoatmospheric pCO<sub>2</sub> changes associated with oceanic anoxic event 1a (Early Aptian, SE France), *Earth Planet. Sci. Lett.*, *223*, 303–318.
- Herrle, J. O. (2002), Paleoceanographic and paleoclimatic implications on mid-Cretaceous black shale formation in the Vocontian Basin and the Atlantic: Evidence from calcareous nannofossils and stable isotopes, *Tübinger Mikropalaentol. Mitt.*, *27*, 1–114.
- Hochuli, P. A., A. P. Menegatti, H. Weissert, A. Riva, E. Erba, and I. P. Silva (1999), Episodes of high productivity and cooling in the early Aptian Alpine Tethys, *Geology*, *27*, 657–660.
- Huck, S., U. Heimhofer, and A. Immenhauser (2012), Early Aptian algal bloom in a neritic proto-North Atlantic setting: Harbinger of global change related to OAE1a?, *GSA Bull.*, *124*(11–12), 1810–1825.
- Huck, W., A. Holbourn, and M. Moullade (2011), Strontium and carbon-isotope chonostratigraphy of Barremian-Aptian shoal-water carbonates: Northern Tethyan platform drowning predates OAE1a, *Earth Planet. Sci. Lett.*, *304*, 547–558.
- Jenkyns, H. C., and P. A. Wilson (1999), Stratigraphy, paleoceanography and evolution of Cretaceous Pacific guyots: Relics from a greenhouse Earth, *Am. J. Sci.*, *299*, 341–392.
- Keller, C. E., P. A. Hochuli, H. Weissert, S. M. Bernasconi, M. Giorgioni, and T. I. Garcia (2011), A volcanically induced climate warming and floral change preceded the onset of OAE1a (Early Cretaceous), *Palaeoogeogr. Palaoclimatol. Palaeoecol.*, *305*, 43–49.
- Kirby, M. X., T. M. Soniat, and H. J. Spero (1998), Stable isotope sclerochronology of Pleistocene and recent oyster shells (*Crassostrea virginica*), *Palaios*, *13*, 560–569.
- Kleypas, J. A., J. W. McManus, and L. A. B. Menez (1999), Environmental limits to coral reef development: Where do we draw the line?, *Am. Zool.*, *39*, 146–159.
- Kuhnt, W., A. Holbourn, and M. Moullade (2011), Transient global cooling at the onset of early Aptian oceanic anoxic event (OAE) 1a, *Geology*, *39*, 323–326.
- Kump, L. R., and M. A. Arthur (1999), Interpreting carbon-isotope excursions: Carbonates and organic matter, *Chem. Geol.*, *161*, 181–198.
- Lécuyer, C., B. Reynard, and F. Martineau (2004), Stable isotope fractionation between mollusc shells and marine waters from Martinique Island, *Chem. Geol.*, *213*, 293–305.
- Liesa, C. L., A. R. Soria, N. Melendez, and A. Melendez (2006), Extensional fault control on the sedimentation patterns in a continental rift basin: El Castellar Formation, Galve, sub-basin, Spain, *J. Geol. Soc. London*, *163*, 487–498.
- Lirman, D., B. Orlando, S. Macia, D. Manzello, L. Kaufman, P. Biber, and T. Jones (2003), Coral communities of Biscayne Bay, Florida and adjacent offshore areas: Diversity, abundance, distribution, and environmental correlates, *Aquat. Conser. Mar. Freshwater Ecosyst.*, *13*, 121–135.
- Masse, J.-P. (1993), Valanginian-Early Aptian carbonate platforms from Provence, southeastern France, in *Cretaceous Carbonate Platforms: An Overview*, *Am. Assoc. of Petrol. Geol., Mem.*, vol. 56, edited by J. A. Simo, R. W. Scott, and J.-P. Masse, pp. 363–374, AAPG, Tulsa, Okla.
- McAnena, A., S. Flögel, P. Hofmann, J. O. Herrle, A. Griesand, J. Pross, H. M. Talbot, J. Rethemeyer, K. Wallmann, and T. Wagner (2013), Atlantic cooling associated with a marine biotic crisis during the mid-Cretaceous period, *Nat. Geosci.*, *6*, 558–651.
- McConnaughey, T. A. (1989a), <sup>13</sup>C and <sup>18</sup>O isotopic disequilibrium in biological carbonates: I. Patterns, *Geochim. Cosmochim. Acta*, *53*, 151–162.

- McConnaughey, T. A. (1989b),  $^{13}\text{C}$  and  $^{18}\text{O}$  isotopic disequilibrium in biological carbonates: II. In vitro simulation of kinetic isotope effects, *Geochim. Cosmochim. Acta*, *53*, 163–171.
- Méhay, S., C. E. Keller, S. M. Bernasconi, H. Weissert, E. Erba, C. Botin, and P. A. Hochuli (2009), A volcanic  $\text{CO}_2$  pulse triggered the Cretaceous Oceanic Anoxic Event 1a and a biocalcification crisis, *Geology*, *37*, 819–822.
- Menegatti, A. P., H. Weissert, R. S. Brown, R. V. Tyson, P. Farrimon, A. Strasser, and M. Caron (1998), High-resolution  $\delta^{13}\text{C}$  stratigraphy through the early Aptian “Livello Selli” of the Alpine Tethys, *Paleoceanography*, *13*, 530–545.
- Moreno-Bedmar, J. A., M. Company, T. Bover-Arnal, R. Salas, G. Delanoy, R. Martínez, and A. Grauges (2009), Biostratigraphic characterization by means of ammonoids of the lower Aptian Oceanic Anoxic Event (OAE 1a) in the eastern Iberian Chain (Maestrat Basin, eastern Spain), *Cretaceous Res.*, *30*, 864–872.
- Ogg, J. G., G. Ogg, and F. M. Gradstein (2008), *The Concise Geologic Time Scale*, 184 pp., Cambridge Univ. Press, Cambridge.
- Parkinson, D., G. B. Curry, M. Cusack, and A. E. Fallick (2005), Shell structure, patterns and trends of oxygen and stable isotopes in modern brachiopod shells, *Chem. Geol.*, *219*, 193–235.
- Pucéat, E., C. Lecuyer, S. M. F. Sheppard, G. Dromart, S. Reboulet, and P. Grandjean (2003), Thermal evolution of Cretaceous Tethyan marine waters inferred from oxygen isotope composition of fish tooth enamels, *Paleoceanography*, *18*(2), 1029, doi:10.1029/2002PA000823.
- Ruppert, D., M. P. Wand, and R. J. Carroll (2003), *Semiparametric Regression, Cambridge Ser. in Stat. and Probab. Math.*, vol. 12, 386 pp., Cambridge Univ. Press, Cambridge.
- Salas, R., and A. Casas (1993), Mesozoic extensional tectonics, stratigraphy and crustal evolution during the Alpine cycle of the eastern Iberian basin, *Tectonophysics*, *228*, 33–55.
- Salas, R., C. Martín-Closas, X. Querol, J. Guimerà, and E. Roca (1991), Evolución tectonosedimentaria de las cuencas del Maestrazgo y Aliaga-Penyagolosa durante el Cretácico Inferior, in *El Cretácico Inferior del Nordeste de Iberia*, pp. 15–47, Publicacions Universitat de Barcelona, Barcelona, Spain.
- Schöne, B. R., A. D. F. Castro, J. Fiebig, S. D. Houk, W. Oschmann, and I. Kröncke (2004), Sea surface water temperatures over the period 1884–4983 reconstructed from oxygen isotope ratios of a bivalve mollusk shell (*Antarctica islandica*, southern North Sea), *Paleoogeogr. Palaeoclimatol. Palaeoecol.*, *212*, 215–232.
- Shöne, B. R., and D. P. Gillikin (2013), Unraveling environmental histories from skeletal diaries—Advances in sclerochronology, *Paleoogeogr. Palaeoclimatol. Palaeoecol.*, *273*, 1–5.
- Schudack, U., and M. Schudack (2009), Ostracod biostratigraphy in the Lower Cretaceous of the Iberian chain (eastern Spain), *J. Iber. Geol.*, *35*(2), 141–168, Madrid.
- Skelton, P. W., and E. Gili (2012), Rudists and carbonate platforms in the Aptian: A case study on biotic interactions with ocean chemistry and climate, *Sedimentology*, *59*, 81–117.
- Stein, M., K. B. Föllmi, S. Westermann, A. Godet, T. Adatte, V. Matera, D. Fleitmann, and Z. Berner (2011), Progressive palaeoenvironmental change during the Late Barremian-Early Aptian as prelude to Oceanic Anoxic Event 1a: Evidence from the Gorgo a Cerbara section (Umbria-Marche basin, central Italy), *Paleoogeogr. Palaeoclimatol. Palaeoecol.*, *302*, 396–406.
- Steuber, T. (1996), Stable isotope sclerochronology of rudist bivalves: Growth rates and late Cretaceous seasonality, *Geology*, *24*, 315–318.
- Steuber, T. (1999), Isotopic and chemical intra-shell variations in low-Mg calcite of rudist bivalves (Mollusca-Hippuritacea): Disequilibrium fractionations and Late Cretaceous seasonality, *Int. J. Earth Sci.*, *88*, 551–570.
- Steuber, T., M. Rauch, J. P. Masse, and M. Malkoč (2005), Low-latitude seasonality of Cretaceous temperatures in warm and cold episodes, *Nature*, *437*, 1341–1344.
- Surge, D., K. C. Lohmann, and D. L. Dettman (2001), Controls on isotopic chemistry of the American oyster, *Crassostrea virginica*: Implications for growth patterns, *Paleoogeogr. Palaeoclimatol. Palaeoecol.*, *172*, 283–296.
- Surge, D. M., K. C. Lohmann, and G. A. Goodfriend (2003), Reconstructing estuarine conditions: Oyster shells as recorders of environmental change, Southwest Florida, *Estuar. Coast. Shelf Sci.*, *57*, 737–756.
- Tejada, M. L. G., K. Suzuki, J. Kuroda, R. Coccioni, J. J. Mahoney, N. Ohkouchi, T. Sakamoto, and Y. Tatsumi (2009), Ontong Java Plateau eruption as a trigger for the early Aptian oceanic anoxic event, *Geology*, *37*, 855–858.
- Ullmann, C. V., U. Wiechert, and C. Korte (2010), Oxygen isotope fluctuations in a modern North Sea oyster (*Crassostrea gigas*) compared with annual variations in seawater temperature: Implications for palaeoclimate studies, *Chem. Geol.*, *277*, 160–166.
- Ullmann, C. V., F. Böhm, R. E. M. Rickaby, U. Wiechert, and C. Korte (2013), The Giant Pacific Oyster (*Crassostrea gigas*) as a modern analog for fossil ostreoids: Isotopic (Ca, O, C) and elemental (Mg/Ca, Sr/Ca, Mn/Ca) proxies, *Geochem. Geophys. Geosyst.*, *14*, 4109–4120, doi:10.1002/ggge.20257.
- van Buchem, F. S. P., M. I. Al Hussein, F. Maurer, and H. J. Droste (2010), Barremian-Aptian stratigraphy and hydrocarbon habitat of the Eastern Arabian Plate, Bahrain, *GeoArabia Spec. Publ.*, *4*, 503–548.
- Vennin, E., and M. Aurell (2001), Stratigraphie séquentielle de l’Aptien du sous-bassin de Galvé (Prov. De Têruel, NE de l’Espagne), *Bull. Soc. Geol. Fr.*, *172*, 397–410.
- Wefer, G., and W. H. Berger (1991), Isotope paleontology: Growth and composition of extant calcareous species, *Mar. Geol.*, *100*, 207–248.
- Weissert, H., and E. Erba (2004), Volcanism,  $\text{CO}_2$  and palaeoclimate: A Late Jurassic-Early Cretaceous carbon and oxygen isotope record, *J. Geol. Soc.*, *161*, 695–702.
- Weissert, H., A. Lini, K. B. Föllmi, and O. Kuhn (1998), Correlation of Early Cretaceous carbon isotope stratigraphy and platform drowning events: A possible link?, *Paleoogeogr. Palaeoclimatol. Palaeoecol.*, *137*, 189–203.
- Zhou, J., C. J. Poulsen, D. Pollard, and T. S. White (2008), Simulation of modern and middle Cretaceous marine  $\delta^{18}\text{O}$  with an ocean-atmosphere general circulation model, *Paleoceanography*, *23*, PA3223, doi:10.1029/2008PA001596.